FAPP2, cilium formation, and compartmentalization of the apical membrane in polarized Madin–Darby canine kidney (MDCK) cells

Otilia V. Vieira*†, Katharina Gaus*‡, Paul Verkade*, Joachim Fullekrug§, Winchil L. C. Vaz¶, and Kai Simons*‖

*Max Planck Institute for Molecular Cell Biology and Genetics, D-01307 Dresden, Germany; §University of Heidelberg, D-69120 Heidelberg, Germany; and ¶Departamento de Química, Universidade de Coimbra, 3004-535 Coimbra, Portugal

Contributed by Kai Simons, September 22, 2006

We have analyzed the role of the phosphatidylinositol-4-phosphate adaptor protein-2 (FAPP2), a component of the apical transport machinery, in cilium formation in polarized Madin–Darby canine kidney (MDCK) cells. We show that ciliogenesis is defective in FAPP2 knockdown cells. Furthermore, by using fluorescence recovery after photobleaching studies of domain connectivity and the generalized polarization spectra of Laurdan, we demonstrate that FAPP2 depletion impairs the formation of condensed apical membrane domains. Laurdan staining also revealed that the ciliary membrane has a highly condensed bilayer domain at its base that could function as a fence to separate the ciliary membrane from the surrounding apical membrane. These results indicate that the compartmentalization of the apical membrane in MDCK cells into the ciliary membrane and the surrounding membrane depends on the balance of raft and nonraft domains.

ciliogenesis | diffusion barriers | rafts

Epithelial cell polarization involves a complex interplay between cues from the extracellular matrix and from cell–cell contacts. Together, these cues lead to the establishment of a basal pole that transmits signals to the microtubule and actin networks (1). This reorganization is accompanied by polarization of the secretory and endocytic apparatus and culminates in the formation of the two cell-surface domains, separated by the junctional complex formed between adjacent epithelial cells. The final stage in the polarization process is the outgrowth of a primary cilium from the apical surface (2). The cellular mechanisms responsible for polarizing the cell surface, installation of the cell–cell junctions, and ciliary biogenesis are still poorly understood.

The primary cilium is a hair-like process that protrudes from the center of the apical membrane (3, 4). Ciliogenesis is initiated from the subapical centriole that forms a basal body, generating an axoneme composed of microtubules and associated proteins. The cilium is surrounded by a membrane that is continuous with the apical membrane but with a different composition. This ciliary membrane has been found to host membrane proteins not present in the apical membrane, such as polycystin 1 and 2, which are implicated in polycystic kidney disease (5). How the ciliary membrane is generated and how its protein constituents are delivered by the biosynthetic membrane traffic machinery is not known.

The sorting and delivery machinery that supplies the apical membrane with proteins and lipids is being intensively studied. Several proteins involved have been identified. One such protein is the phosphatidylinositol-4-phosphate adaptor protein-2 (FAPP2), a peripheral membrane protein with a pleckstrin homology domain that specifically interacts with phosphatidylinositol-4-phosphate [PI (4)P] (6). Loss-of-function studies in polarized Madin–Darby canine kidney (MDCK) cells have shown that FAPP2 is specifically involved in the apical transport of newly synthesized proteins (7). In this article, we have continued these studies and shown that FAPP2 depletion impairs the outgrowth of primary cilia in MDCK cells, most likely by defective apical transport and the resulting changes in apical membrane properties. Moreover, we demonstrated the presence of a condensed lipid zone at the base of the cilium. This zone could function as a diffusion barrier to maintain the unique protein composition of the ciliary membrane.

Results

FAPP2 Deficiency Delays Cilium Formation in FAPP2-Knockdown (KD) MDCK Cells. FAPP2, a protein that associates with the Golgi through the binding of its pleckstrin homology domain to PI (4)P, is part of the apical transport machinery in MDCK cells (7). The delivery of apical cargo is retarded upon depletion of FAPP2, providing us with a tool to study the effects of inhibited biosynthetic delivery on the organization of the apical membrane. We first analyzed the formation of the primary cilium, one of the most conspicuous features of the apical membrane. The role of FAPP2 in ciliogenesis of filter-grown MDCK cells and in Matrigel MDCK cell cysts was studied by RNAi using a retrovirus-mediated RNAi system. When visualized by immunofluorescence (IF) with antiacetylated β-tubulin antibodies, the primary cilia were seen projecting from the apical surface of filter-grown MDCK (Fig. 1). Four days after seeding FAPP2-KD cells, >70% of these cells failed to grow primary cilia (Fig. 1 *B* and *C*, white bar), whereas >60% of WT control cells treated with empty retrovirus (Fig. 1 *A* and *C*, black column) or WT cells treated with RNAi directed against phosphatidylinositol-4-phosphate adaptor protein-1 (FAPP1; results not shown) showed normal full-length primary cilia. Similar results were observed in Matrigel cysts after 7 days of culture (Fig. 1 *D–F*). However, the effect of FAPP2 depletion in cilium formation could eventually be overcome with time in filter-grown cultures of FAPP2-KD cells, which showed apparently normal cilia (judged by IF staining) after 6–7 days. In contrast, FAPP2-KD cysts did not show cilium formation even 7 days after seeding.

FAPP2 Depletion Causes a Restricted Accumulation of Subapical Vesicles and Formation of Collapsed Lumena in Matrigel Cysts. Next, we examined other characteristics of epithelial cell polarization that could account for the striking delay of ciliogenesis in the absence of FAPP2. The effect of FAPP2 depletion on cell

Author contributions: O.V.V. and K.S. designed research; O.V.V., K.G., P.V., J.F., and W.L.C.V. performed research; O.V.V. contributed new reagents/analytic tools; O.V.V., K.G., P.V., J.F., W.L.C.V., and K.S. analyzed data; and O.V.V. and K.S. wrote the paper.

The authors declare no conflict of interest.

Abbreviations: EGFR, epidermal growth factor receptor; FGL, Forssman glycolipid; FRAP, fluorescence recovery after photobleaching; GP, generalized polarization; IF, immunofluorescence; KD, knockdown; MDCK, Madin–Darby canine kidney; PI(4)P, phosphatidylinositol 4-phosphate.

See Commentary on page 18383.

†Present address: Centro de Neurociencias e Biologia Celular, Universidade de Coimbra, 3000 Coimbra, Portugal.

‡Present address: Center for Vascular Research at the School of Medical Sciences, University of New South Wales, Sydney 2052 NSW, Australia.

‖To whom correspondence should be addressed. E-mail: simons@mpi-cbg.de.

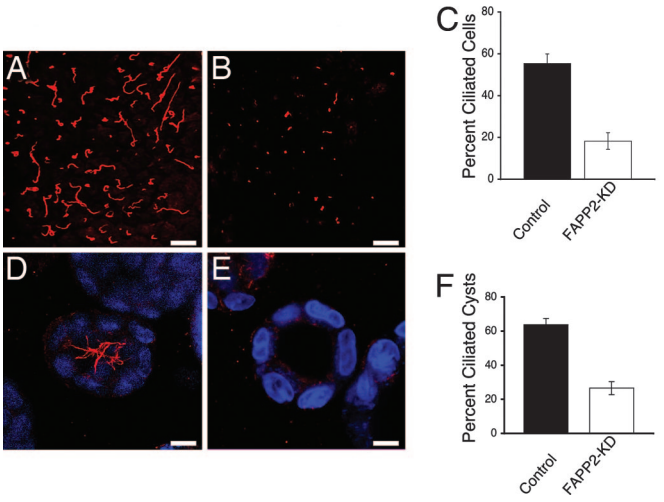

Fig. 1. FAPP2 is required for ciliogenesis. Primary cilia on filter-grown MDCK cells and on Matrigel cysts. MDCK cells were grown at confluence for 4 or 7 days on Transwell filters (*A–C*) or Matrigel (*D–F*), respectively, and then processed for IF. Cilia were labeled with an antibody to acetylated tubulin to reveal the ciliary axoneme (*A*, *B*, *D*, and *E*, red) and with DAPI to stain the nucleus (*D* and *E*, blue). (*C* and *F*) Quantification of the effect of FAPP2 depletion on cilia formation on filter-grown MDCK cells and cysts, respectively. Data are means ± SE of three separate experiments. *A* and *D* and black columns in *C* and *F* are controls. *B* and *E* and white columns in *C* and *F* are KD cells. (Scale bars, 10 μm.)

polarization was assessed by investigating the cellular distribution, as a function of time, of apical (podocalyxin) apical and subapical (galectin-3) and basolateral (β-subunit of Na^+K^+-ATPase or gp58 (8) and E-cadherin) markers by IF. No differences in the localization of the endogenous apical and basolateral markers were observed 1 day after seeding control (Fig. 2 *A* and *E*) and FAPP2-KD cells (Fig. 2 *B* and *F*) at the same density on Transwell filters. In contrast, galectin-3 distribution was different in FAPP2-KD (Fig. 2*D*) when compared with control cells (Fig. 2*C*), being subapical in control and both subapical and basal in FAPP2-KD cells. In addition, the FAPP2-KD cell monolayer (Fig. 2*B*) was less even, and the cells

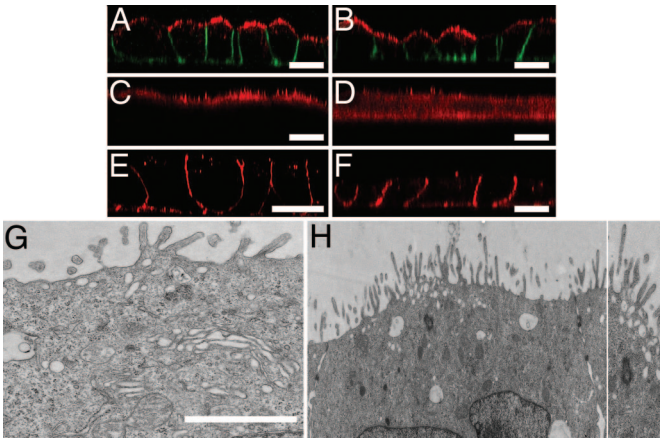

Fig. 2. FAPP2 depletion causes an accumulation of subapical vesicles. (*A–F*) Distribution of apical (*A* and *B*, podocalyxin, red), subapical (*C* and *D*, galectin-3), and basolateral (*A* and *B*, green, E-cadherin; *E* and *F*, gp58) markers in control (*A*, *C*, and *E*) and FAPP2-KD cells (*B*, *D*, and *F*). (*G* and *H*) Electron micrographs of control (*G*) and KD cells (*H*). *H* also shows the zoom in of the microtubule-organizing center region. The cells were grown at confluence for 1 day on Transwell filters and then processed for indirect immunofluorescence or for EM. (Scale bars, 10 μm.)

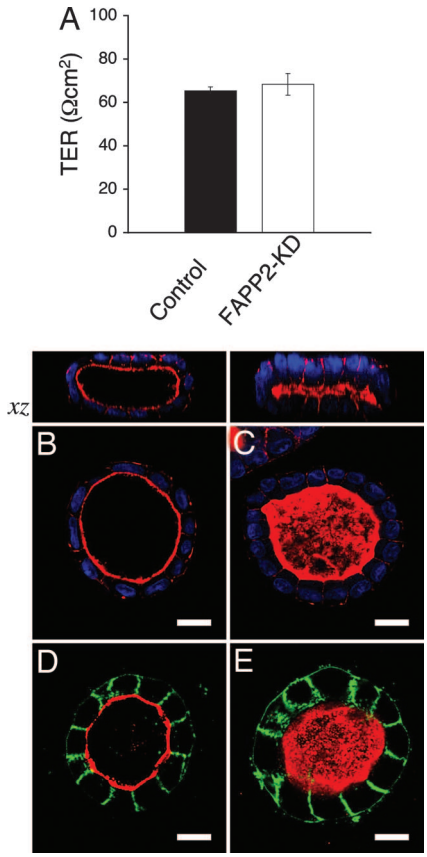

Fig. 3. FAPP2 depletion induces morphological changes in the apical lumen of cysts. (*A*) The transepithelial resistance (TER, graph) was determined in filter-grown cells as described in *Materials and Methods*. The cells were seeded on polycarbonate filters for 4 days. The black column corresponds to control, and the white column corresponds to KD cells. Data are means ± SE of three separate experiments. (*B–E*) KD and control cells were suspended in Matrigel and cultured in the matrix for 4–7 days. The cysts were fixed and processed. Confocal sections passing through the middle of each cyst are shown. Whereas >60% of the KD cells (*C*) had formed cysts with a collapsed apical lumen, as visualized by actin staining with TRITC-phalloidin (red) and nuclear staining with DAPI (blue), only 20% of control cells (*B*) displayed a collapsed lumen. Apical (podocalyxin, red) and basolateral (gp58, green) distribution in control (*D*) and FAPP2-KD (*E*) cells is shown. (Scale bars, 10 μm.)

were shorter than in controls (Fig. 2*A*). Ultrastructural analysis revealed that FAPP2 depletion caused a striking but transient accumulation of vesicular structures in the vicinity of the microtubule organizing center (Fig. 2*H*), resembling a "traffic jam." These vesicular structures disappeared in the FAPP2-KD cells 3–4 days after seeding and were not observed in control (Fig. 2*G*) or FAPP1-KD cells at any time (results not shown). When control and FAPP2-KD cells were grown to confluence on Transwell filters for long periods of time (>4 days), no differences between these cells could be observed (data not shown). After 4 days, the transepithelial resistance in control and KD cells was also similar (Fig. 3*A*), indicating that tight junctions were fully functional.

Next, we analyzed how control and FAPP2-KD cells (Fig. 3 *B–E*) polarize when grown in 60% Matrigel for 4–7 days to form cysts. Cells were double labeled with rhodamine–phalloidin and DAPI (Fig. 3*B*, control and Fig. 3*C*, FAPP2-KD) or with podocalyxin and gp58 antibodies (Fig. 3*D*, control and Fig. 3*E*, FAPP2-KD). As observed in the case of filter-grown cells, apical/basal polarity was not affected in the cyst-grown cells because podocalyxin and gp58 are only ob-

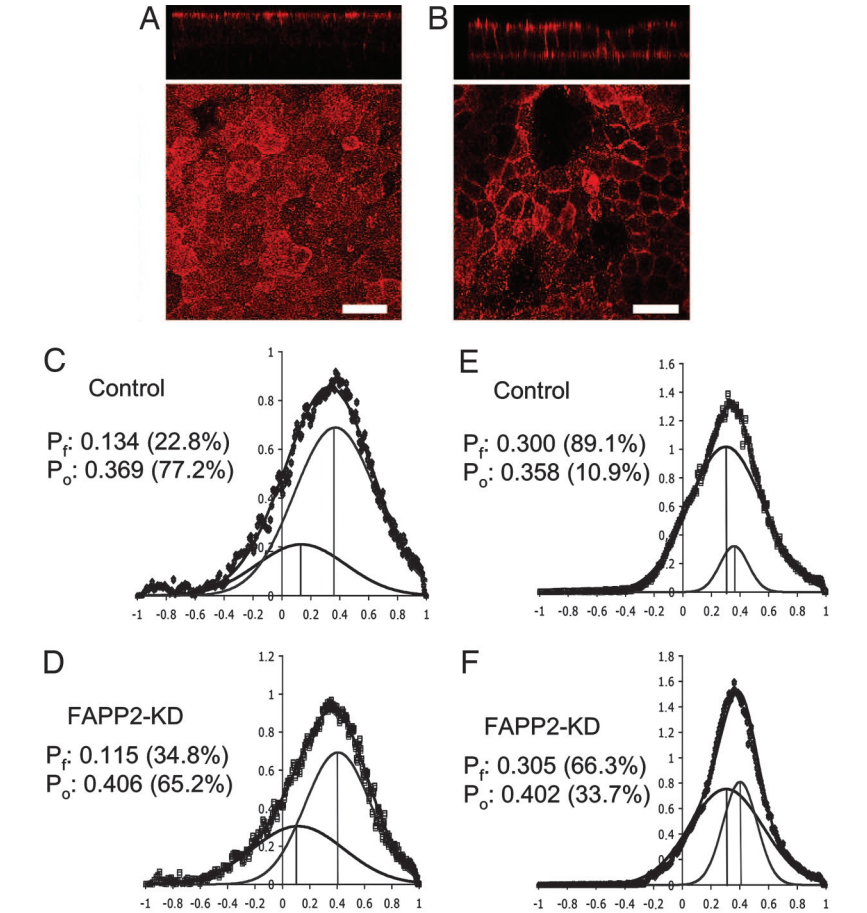

G

n(x, y)	(*D* ± Std.Dev.) [$\mu m^2 s^{-1}$]	Fraction recovered ± Std.Dev.
EGFR-TMD-GFP-Cont. *(10, 7)*	0.007 ± 0.005	0.80 ± 0.17
EGFR-TMD-GFP-KD *(10, 9)*	0.007 ± 0.005	0.95 ± 0.13
LAT-TMD-GFP-Cont. *(3, 14)*	0.029 ± 0.013	1.02 ± 0.06
LAT-TMD-GFP-KD *(3, 10)*	0.034 ± 0.018	1.02 ± 0.05

Fig. 4. FAPP2 depletion changes the physical state of the apical plasma membrane. (*A* and *B*) Forssman glycolipid distribution in filter-grown control (*A*) and KD (*B*) cells. (Scale bars, 10 μm.) (*C–F*) Control (*C* and *E*) and FAPP-2 KD (*D* and *F*) cells were plated onto coverslips at a density of 100×10^3 per 2 cm^2, grown to confluent monolayers for 24 h, Laurdan labeled, and stained for apical marker protein podocalyxin (*C* and *D*) or basolateral marker gp58 (*E* and *F*). The distributions of ≈12 GP images from a single experiment taken at a focal depth corresponding to either apical or basolateral membranes were normalized and fitted to two Gaussian populations (black line through data). The fit yielded in a fluid population (P_f, dark gray) and a more ordered population (P_o, light gray). The mean GP of these populations as well as the coverage of the population (corresponding to the area under the curves) is given in each subpanel. Erfs for *C–F* are 0.0031, 0.0025, 0.0049, and 0.0018, respectively. (*G*) Table showing the diffusion coefficient, *D*, and the fraction that recovered in FRAP experiments on control and FAPP2-KD cells. Values are presented as averages ± 1 SD for the nonraft marker protein (EGFR-TMD-GFP in blue) and the raft marker protein (LAT-TMD-GFP in red). A circular spot of 4-μm^2 area was bleached on the apical membrane, and the fluorescence recovery due to diffusion was recorded at room temperature. The raw experimental data were corrected for bleaching during the recording, normalized, and fitted to a 2D diffusion model (12, 13). The number of FRAP curves *n* used for the theoretical analysis is given by $n = xy$, where *x* is the number of independent experiments, and *y* is the average number of cells examined per experiment.

served on the apical and basolateral domains, respectively, in both control (Fig. 3*D*) and FAPP2-KD cells (Fig. 3*E*). However, a strong effect on the lumen shape was observed in FAPP2-KD cells. Most of the control MDCK cells (81 ± 4.2%) formed cysts with an approximately spherical lumen (Fig. 3*B*). In contrast, FAPP2-KD cells exhibited a "collapsed" lumen, with small *xz* diameter (Fig. 3*C*, *xz*). This abnormal lumen was observed in most of the cysts (60 ± 7.0%), and it was not observed in FAPP1-KD cells, indicating that this effect was specific to FAPP2 depletion. The morphological characteristics of the cyst lumina were maintained in both control and FAP2-KD cells even 7 days after seeding.

Properties of the Apical Membrane Are Different in WT and FAPP2-KD Cells. As shown above, FAPP2-depletion does not seem to result in mislocalization of the apical (podocalyxin) and basolateral (gp58 and E-cadherin) membrane proteins. The lack of FAPP2 could, however, result in mislocalization of raft lipids. We therefore examined the effects of FAPP2-depletion on the distribution of the Forssman glycolipid (FGL), a raft lipid. FGL is distributed apically in control (Fig. 4*A*), whereas, in FAPP2-KD cells (Fig. 4*B*), FGL is also observed basolaterally.

To further analyze differences between the apical membrane in control and FAPP2-KD cells, we examined the extent of condensation of the plasma membrane in WT and FAPP2-KD cells using

two biophysical techniques: (*i*) generalized polarization spectra of Laurdan-stained membranes and (*ii*) condensed phase connectivity using fluorescence recovery after photobleaching (FRAP).

The emission spectrum of Laurdan is sensitive to the degree of condensation (ordering) of its lipid bilayer environment. This sensitivity is best exploited by using the generalized polarization (GP) spectrum of the dye and permits defining the mass fraction of ordered phases in both artificial membranes with liquid-ordered/liquid-disordered phase coexistence (9) and in cells (10). Cells (WT and FAPP2-KD) were labeled with Laurdan and apical/basolateral markers, and GP values were determined at the focal depth corresponding to apical or basolateral membranes. FAPP2 depletion resulted in 12% reduction of condensed lipid domains in the apical membrane (Fig. 4*D*) and 23% increase in condensed domains in the basolateral membranes (Fig. 4*F*) when compared with control cells (Fig. 4 *C* and *E*).

We have recently shown that raft and nonraft proteins display different diffusion characteristics in the apical membrane of MDCK and Caco2 cells (11). The data suggested that the apical membrane behaves as a percolating "raft phase" at 25°C. We used the same methodology as before to examine the diffusion of two proteins in the apical membranes of WT and FAPP2-KD MDCK cells. The proteins examined were LAT-TMD-GFP (a raft marker) and EGFR-TMD-GFP (a nonraft marker). In the previous work, it was shown that the former diffuses relatively fast (lateral diffusion coefficient, $D \approx 0.02\ \mu m^2 \cdot s^{-1}$), with complete fluorescence recovery at "infinite" times after the photobleaching event, whereas the latter diffuses much more slowly ($D \approx 0.007\ \mu m^2 \cdot s^{-1}$), with only partial (≈80%) recovery. Our results with LAT-TMD-GFP were indistinguishable in both WT and FAPP2-KD cells (see Fig. 4*G*, red color), being identical to the results reported from this laboratory (11). The nonraft marker EGFR-TMD-GFP, however, showed less confined diffusion behavior in FAPP2-KD cells than it did in control cells ($P = 0.000$) (see Fig. 4*G*, blue color; and see Fig. 6, which is published as supporting information on the PNAS web site). These results were similar to those obtained in cells polarized for 3 or 5 days. We conclude that, whereas the "nonraft phase" in the apical membranes of WT MDCK cells is discontinuous at 25°C, as reported, it is changed in the FAPP2-KD cells. Altogether, these results suggest that FAPP2 depletion slightly changed the apical/basolateral lipid raft balance.

The Ciliary Membrane Has a Condensed Lipid Zone at the Base, Excluding an Exogeneously Expressed GPI-Anchored Protein. The composition and physical properties of cilia membranes were assessed by IF and Laurdan fluorescence, respectively. All experiments were conducted on WT MDCK cells grown on polycarbonate filters for 4 days after confluence to allow full epithelial polarization and cilia formation. The cellular distribution of FGL was compared with that of acetylated β-tubulin. FGL was observed apically as well as in cilia (Fig. 5*B*). In cilia it colocalized with acetylated β-tubulin (Fig. 5*A*). In contrast, expression of an apical GPI-anchored protein (YFP-GL-GPI or FP-GPI) did not enter the ciliary membrane (Fig. 5 *D–F*). In fact, FP-GPI was excluded from an area of 1.2- to 1.8-μm diameter at the center of the apical membrane (Fig. 5*E*) that corresponds to the site of outgrowth of the primary cilium (Fig. 5*F*). This central area devoid of FP-GPI staining is 4–9 times larger in diameter than the cilium (≈0.2- to 0.3-μm diameter). A lectin, galectin-3, could also be identified to be surrounding the exclusion area in the center of the apical membrane (Fig. 5 *H–I*). Galectin-3 depletion using a retrovirus-mediated RNAi system and 21-nt-long target sequence without significant homology to other known genes, did not change the membrane distribution of FP-GPI (results not shown). It is, therefore, unlikely that FP-GPI exclusion from the center of apical and ciliary membranes is due to galectin-3. Instead, it is possible that the galectin-3 binds to some as yet unidentified component surrounding the exclusion area that creates a diffusion barrier that keeps FP-GPI out of it.

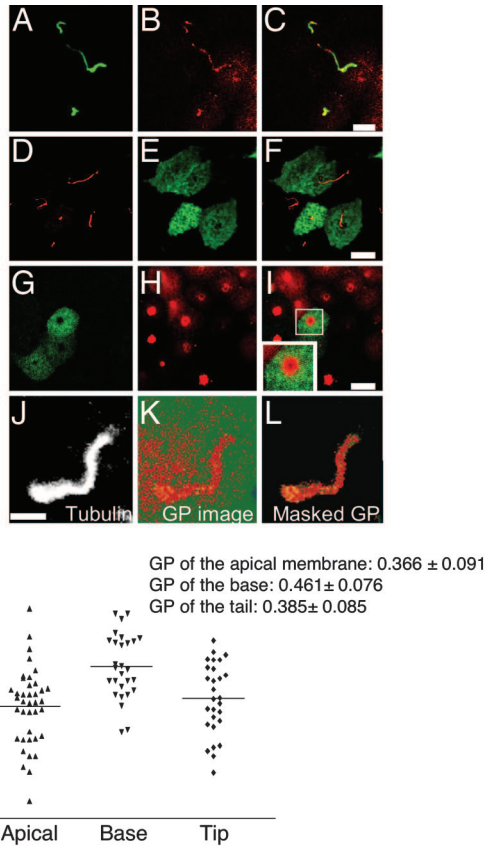

Fig. 5. The ciliary membrane has a condensed lipid domain at its base. (*A*, *D*, and *J*) Primary cilia revealed by using an antibody to acetylated tubulin. (*B*) FGL distribution. (*C*) FGL labels both apical membrane and cilia. (*E* and *G*) YFP-GL-GPI distribution. (*F*) YFP-GL-GPI is excluded from the center of the apical membrane that corresponds to the site of outgrowth of the primary cilium (red). (*H*) Galec tin-3 distribution. (*I*) Galectin-3 is confined to a subdomain of the apical membrane surrounding the site of outgrowth of the primary cilium. (*J–L*) Filter-grown MDCK cells were fixed and simultaneously imaged for the Laurdan intensity and acetylated tubulin. For Laurdan intensity, images were converted to GP images (*K*) as described in *Materials and Methods*. (Scale bars, 10 μm.) (*M*) GP values at apical membrane domain (▲, $n = 39$), base (▼, $n = 28$), and tip (◆, $n = 28$) of cilia were determined for individual images. Means (indicated by horizontal lines) and SDs are indicated in the graph.

To assess the degree of lipid condensation in cilia, MDCK cells were labeled with Laurdan, fixed, and immunostained with antibodies against acetylated β-tubulin. After 30-min incubation at 37°C, Laurdan fluorescence revealed a zone of high GP at the base of the cilium (Fig. 5 *K* and *L*). For quantification, we determined the mean GP at the base and at the tip of cilia and also the membrane area adjacent to cilia. As shown in Fig. 5*M*, the base of cilia is more condensed than the surrounding apical membrane ($P < 0.001$) and the tip ($P < 0.05$), which is similar to the apical membrane (Fig. 5*M*). These results show that the ciliary membrane has a basal zone with condensed lipids that could be functioning as a fence for diffusion.

Discussion

The apical membrane of epithelial cells has to form a barrier that protects the epithelial-cell layer from damage from the outside. Thus, a lipid composition that allows the formation of a more densely packed bilayer than is normally the case would be ideal for this purpose. Indeed, the apical membrane of epithelial cells is known to be enriched in sphingolipids that, together with choles-

terol, can form a liquid-ordered phase in simplified model membranes (14). We have recently demonstrated that the apical membrane of polarized MDCK cells displays the properties of a connected (percolating) raft phase at 25°C in which isolated domains of the nonraft phase are dispersed (11). These experiments were based on analyzing the diffusion characteristics of raft- and nonraft-protein probes. In the apical membrane at 25°C, the raft proteins displayed diffusion behavior typical of a continuous lipid phase, whereas the nonraft probes were impeded in their diffusion, most likely because of discontinuous pools of nonraft phase. However, raising the temperature to 37°C was sufficient to break down the percolating raft phase (11). Thus, the apical membrane of MDCK cells has a percolation threshold (continuous [rarrrow] discontinuous raft phase) between 25°C and 37°C, and a temperature shift is sufficient to change the balance.

In this work, we tried to perturb the formation of the apical membrane by FAPP2 depletion. We had already shown that FAPP2 is involved in the transport of apically targeted cargo (7). Here, we demonstrated that FAPP2 depletion causes a shift in the lipid phase balance in the apical membrane of MDCK cells, shown by employing the same FRAP approach as previously. At 25°C in FAPP2-KD cells, the diffusion of nonraft marker proteins was not as confined as in control cells but displayed diffusion, characteristic of a percolating phase. Thus, there is less of the condensed raft phase in FAPP2-KD cells than in WT cells. GP spectra of the fluorescent probe, Laurdan, a dye that can be used to monitor the amount of condensed lipid phases in cell membranes (15), confirmed this finding. In keeping with the FRAP data, GP spectra of Laurdan-stained cells showed a slight but significant decrease (≈12%) in condensed lipid bilayer in the apical membranes of FAPP2-KD cells.

A striking phenotypic change in MDCK cells caused by FAPP2 depletion was the retarded formation of the primary cilium. This change was preceded by a transient accumulation of subapical vesicles in the vicinity of the subapical centrosome. The function of these vesicles is not clear; they could be involved in apical membrane biogenesis and/or contribute to the formation of the ciliary membrane. This latter membrane has been shown to be generated by fusion of vesicles around the centriole (16), a process that could be impaired in FAPP2-KD cells. We could not detect any polarization defect in FAPP2-KD cells in what concerns apical and basolateral marker protein distribution. However, the normally apical domain glycolipid, FGL, appears in both apical and basolateral domains of these cells. This abnormal distribution could be caused by a disturbed delivery of raft lipids to the apical membrane. In keeping with the observed changes in apical membrane behavior in the FRAP and the Laurdan experiments, FAPP2 depletion could result in a changed lipid composition in the apical membrane. This postulated shift in lipid composition could be sufficient to impair ciliogenesis. This finding has to be experimentally verified by direct lipid analysis of the purified apical membrane.

A most exciting by product of the Laurdan measurements was the identification of a zone at the base of the cilium that had the highest GP index measured until now. The surrounding ciliary and apical membranes both had similar but lower GP indices. Interestingly, overexpressed GPI-anchored proteins containing YFP as ectodomain were delivered to the apical membrane but excluded from the ciliary membrane. Many apical proteins, including podocalyxin (3), do show a conspicuous absence from the middle of the apical membrane, the area from which the cilium protrudes. Several cystoproteins, implicated in polycystic kidney disease, including the integral membrane proteins polycystin 1 and 2, are localized in the ciliary membrane but excluded from the surrounding apical membrane (5). Therefore, the basal ciliary zone could function as a diffusion barrier. Early freeze–fracture EM studies by Gilula and Satir (17) demonstrated a row of intramembranous particles resembling a "necklace" at the base of the cilium. The molecular identity of these particles remains unknown. We showed that a cytoplasmic lectin, galectin-3 (18), forms a ring outlining the exclusion zone. Because depletion of galectin-3 did not abolish the diffusion barrier, it cannot be galectin-3 *per se* but other membrane proteins to which galectin-3 binds that must be responsible for forming a "fence" at the ciliary base.

Diffusion barriers have also been described in polarized yeast cells and suggested to be responsible for the compartmentalization of intracellular organelles. For example, Luedeke *et al.* (19) found in budding yeast the existence of a septin-dependent diffusion barrier in the endoplasmic reticulum during cytokinesis.

An intriguing issue is how integral cystoproteins are delivered to the ciliary membrane. Protein packets are transported up the axoneme by dynein motors (20). But it is unclear where delivery of transport vesicles takes place. In photoreceptor cells, newly synthesized rhodopsin is transported to the photosensitive outer segment, where the proteins are incorporated into membrane discs to function in light reception (21, 22). This transport is mediated by a connecting cilium, an outgrowth of the inner segment, a plasma membrane domain equivalent to the apical membrane in epithelial cells. There is evidence for the delivery of the carrier vesicles that transport rhodopsin from the trans-Golgi network to the inner segment, where they fuse with the specialized site surrounding the cilium (23). Rhodopsin then diffuses along the ciliary membrane, perhaps propelled into the outer segment by cytoskeletal motors (24).

Similarly, specialized membrane carriers could deliver proteins to the primary cilium in epithelial cells by docking at the base of the primary cilium. Exocyst proteins have been localized to the base (25), and they could be part of the delivery and receiving machinery (26, 27). Little is known about the trafficking route that newly synthesized ciliary membrane proteins use after leaving the Golgi complex. We assume that FAPP2 is not involved in ciliary protein transport but is involved in transport of raft lipids to the apical membrane. Impaired ciliogenesis may come about from disturbed raft lipid delivery.

To elucidate the mechanisms involved in generating and maintaining the apical pole of epithelial cells fenced in by the junctional complexes is, in itself, a formidable challenge. Now, we know that we have to include the formation of the cilium in the morphogenesis of the apical membrane, further complicating the task.

Materials and Methods

Reagents and Antibodies. Cell culture media were from Invitrogen (Carlsbad, CA) or PAA Laboratories (Pasching, Austria). TRITC-phalloidin and Laurdan were from Molecular Probes (Eugene, OR). The hybridoma cell line 3F2 secreting antibodies against gp135 or podocalyxin (3, 28) was provided by G. Ojakian (State University of New York Downstate Medical Center, Brooklyn, NY) and A. Muesch (Cornell University, Ithaca, NY). The monoclonal anti-Forssman antibody was from culture supernatants of American Type Culture Collection (Manassas, VA) TIB 121 (29). Antibodies against E-cadherin (30) and gp58 (β-subunit of Na^+K^+-ATPase) (8, 31) were been raised in our laboratory. Other antibodies used were as follows: mouse anti-MAC-2 (galectin-3) (Cedar Lane Laboratories, Hornby, ON, Canada) and mouse antiacetylated tubulin (Sigma, St. Louis, MO). Polyclonal anti-podocalyxin antibody was raised against the cytoplasmic tail of podocalyxin (CDNLAKDDLDEEEDTHL). Fluorochrome-conjugated secondary antibodies were from Jackson ImmunoResearch (West Grove, PA). All of the other reagents were from Sigma.

Cell Culture and Transfection. MDCK cells were grown on 12-mm Transwell polycarbonate filters (Corning Costar, Corning, NY) in MEM with 10% FCS. For polarization analysis, 2.5×10^5 cells were seeded onto filters and analyzed by IF after 1 or 4 days of growth. For cyst formation, 25 μl of cell suspension containing 5×10^4 cells

were mixed with 50 μl of Matrigel (Becton Dickinson, Franklin Lakes, NJ), 12-μl drops were placed into 2-cm^2 wells and allowed to solidify for 1 h at 37°C before culture medium was added.

MDCK cells were transfected by electroporation [5 μg of DNA for 10^6 cells, Amaxa (Gaithersburg, MD) technology] before seeding onto filters or, for expression of YFP-GL-GPI, infected with replication-deficient adenovirus (Qbiogene, Heidelberg, Germany) 1 day before the experiment.

RNAi and DNA Constructs. Hairpin-forming oligonucleotides targeting a sequence of 19–21 nucleotides (the targeting sequences are supplied in ref. 7) were incorporated into retroviruses as described (32). With all target sequences, depletion of mRNA levels reached 85–95% (real-time PCR), and protein levels were down to 10% at day 4 after transduction, both for FAPP1 and FAPP2 as observed (7).

YFP-GL-GPI, epidermal growth factor receptor (EGFR)-TMD-GFP, and LAT-TMD-GFP expression constructs have been described (11, 33, 34).

Measurement of Transepithelial Resistance. The transepithelial resistance of the control and FAPP2-KD monolayers was measured by using an EVOM epithelial voltohmmeter (World Precision Instruments, Hamden, CT) with a pair of chopstick electrodes.

Immunofluorescence, Confocal Microscopy, and EM. IF was performed as described (35). Fixed stained sample cells were analyzed by confocal microscopy using a LSM 510 laser scanning confocal microscope (Zeiss, Oberköchen, Germany) with a ×100 oil-immersion objective. Digital images were prepared by using Adobe Photoshop and Adobe Illustrator (Adobe Software, Mountain View, CA).

Laurdan intensity images were obtained with an inverted microscope (Bio-Rad, Hercules, CA) under excitation at 800 nm with a Verdi/Mira 900 multiphoton laser system. Laurdan intensity images were recorded simultaneously with emission in the range of 400–460 nm and 470–530 nm. Microscopy calibrations were performed as described (36). For all images, a ×63 oil objective, $N_A = 1.3$, was used, and imaging was performed at room temperature.

Standard Epon embedding of filter-grown cells was performed as described (37, 38).

Image analysis. The generalized polarization GP, defined as

$$GP = \frac{I_{(400-460)} - I_{(470-530)}}{I_{(400-460)} + I_{(470-530)}}, \quad [1]$$

was calculated for each pixel by using the two Laurdan intensity images with the software WIT (36). GP images were pseudocolored in Adobe Photoshop. GP distributions were obtained from the histograms of the GP images, normalized (sum = 100), and fitted to two Gaussian distributions by using the nonlinear fitting algorithm (Excel; Microsoft, Redmond, WA). The quality of the fit was determined by an error function (ERF)

$$ERF = \frac{\sum_i [y(i)_{obs} - y(i)_{fit}]^2}{\sum_i y(i)^2_{obs}}, \quad [2]$$

where $y(i)_{obs}$ and $y(i)_{fit}$ are the experimental and calculated values, respectively. A fit is regarded as excellent when ERF < 0.01.

To determine GP distribution at apical and basolateral membranes, Laurdan intensity images were recorded at identical focal depth as the peak intensity of podocalyxin and gp58, respectively. Marker proteins were immunostained with Cy3-conjugated secondary antibodies. To determine GP values of cilia, tubulin staining was used to identify cilia, and the GP value of the bases and the tails of the cilia and membranes adjacent to cilia was determined separately.

FRAP Measurements and Analysis. The FRAP measurements and data analysis were performed as described by Meder *et al.* (11) in polarized WT and FAPP2-KD MDCK cells expressing (EGFR)-TMD-GFP or LAT-TMD-GFP.

Statistics. Means and standard deviation of two populations were compared with unpaired Student's t tests assuming unequal variances. For multiple comparisons, one-way ANOVA with Tukey's post hoc testing was performed assuming Gaussian distributions (PRISM).

We thank S. Dienel for technical assistance and P. Keller (Meso Scale Discovery, Dresden, Germany), D. Meder (Max Planck Institute), and M. Yamabhai (Suranaree University of Technology, Nakhorn Ratchasima, Thailand) for cDNA constructs. O.V.V. was a recipient of a Marie Curie postdoctoral fellowship. This work was supported by SFB-TR13-TPA1 and MPRN-CT-2002-00259 and research grants from the Portuguese Ministry of Sciences and Higher Education through the "Programa Operacional Ciência, Tecnologia, Inovação."

1. Yeaman C, Grindstaff KK, Nelson WJ (1999) *Physiol Rev* 79:73–98.
2. Bacallao R, Antony C, Dotti C, Karsenti E, Stelzer EH, Simons K (1989) *J Cell Biol* 109:2817–2832.
3. Meder D, Shevchenko A, Simons K, Fullekrug J (2005) *J Cell Biol* 168:303–313.
4. Praetorius HA, Spring KR (2005) *Annu Rev Physiol* 67:515–529.
5. Pazour GJ, Witman GB (2003) *Curr Opin Cell Biol* 15:105–110.
6. Godi A, Di Campli A, Konstantakopoulos A, Di Tullio G, Alessi DR, Kular GS, Daniele T, Marra P, Lucocq JM, De Matteis MA (2004) *Nat Cell Biol* 6:393–404.
7. Vieira OV, Verkade P, Manninen A, Simons K (2005) *J Cell Biol* 170:521–526.
8. Fullekrug J, Shevchenko A, Simons K (2006) *BMC Biochem* 7:8.
9. Bagatolli LA, Sanchez SA, Hazlett T, Gratton E (2003) *Methods Enzymol* 360:481–500.
10. Gaus K, Chklovskaia E, Fazekas de St Grothqq B, Jessup W, Harder T (2005) *J Cell Biol* 171:121–131.
11. Meder D, Moreno MJ, Verkade P, Vaz WL, Simons K (2006) *Proc Natl Acad Sci USA* 103:329–334.
12. Axelrod D, Koppel DE, Schlessinger J, Elson E, Webb WW (1976) *Biophys J* 16:1055–1069.
13. Soumpasis DM (1983) *Biophys J* 41:95–97.
14. Simons K, Vaz WL (2004) *Annu Rev Biophys Biomol Struct* 33:269–295.
15. Gaus K, Zech T, Harder T (2006) *Mol Membr Biol* 23:41–48.
16. Sorokin S (1962) *J Cell Biol* 15:363–377.
17. Gilula NB, Satir P (1972) *J Cell Biol* 53:494–509.
18. Dumic J, Dabelic S, Flogel M (2006) *Biochim Biophys Acta* 1760:616–635.
19. Luedeke C, Frei SB, Sbalzarini I, Schwarz H, Spang A, Barral Y (2005) *J Cell Biol* 169:897–908.
20. Rosenbaum JL, Witman GB (2002) *Nat Rev Mol Cell Biol* 3:813–825.
21. Deretic D, Papermaster DS (1993) *J Cell Sci* 106(Pt 3):803–813.
22. Sung CH, Tai AW (2000) *Int Rev Cytol* 195:215–267.
23. Deretic D, Traverso V, Parkins N, Jackson F, Rodriguez de Turco EB, Ransom N (2004) *Mol Biol Cell* 15:359–370.
24. Beech PL, Pagh-Roehl K, Noda Y, Hirokawa N, Burnside B, Rosenbaum JL (1996) *J Cell Sci* 109 (Pt 4):889–897.
25. Rogers KK, Wilson PD, Snyder RW, Zhang X, Guo W, Burrow CR, Lipschutz JH (2004) *Biochem Biophys Res Commun* 319:138–143.
26. TerBush DR, Maurice T, Roth D, Novick P (1996) *EMBO J* 15:6483–6494.
27. Grindstaff KK, Yeaman C, Anandasabapathy N, Hsu SC, Rodriguez-Boulan E, Scheller RH, Nelson WJ (1998) *Cell* 93:731–740.
28. Ojakian GK, Schwimmer R (1988) *J Cell Biol* 107:2377–2387.
29. Willison KR, Stern PL (1978) *Cell* 14:785–793.
30. Gumbiner B, Simons K (1986) *J Cell Biol* 102:457–468.
31. Balcarova-Stander J, Pfeiffer SE, Fuller SD, Simons K (1984) *EMBO J* 3:2687–2694.
32. Schuck S, Manninen A, Honsho M, Fullekrug J, Simons K (2004) *Proc Natl Acad Sci USA* 101:4912–4917.
33. Yamabhai M, Anderson RG (2002) *J Biol Chem* 277:24843–24846.
34. Keller P, Toomre D, Diaz E, White J, Simons K (2001) *Nat Cell Biol* 3:140–149.
35. Fullekrug J, Scheiffele P, Simons K (1999) *J Cell Sci* 112 (Pt 17):2813–2821.
36. Gaus K, Gratton E, Kable EP, Jones AS, Gelissen I, Kritharides L, Jessup W (2003) *Proc Natl Acad Sci USA* 100:15554–15559.
37. Lahtinen U, Honsho M, Parton RG, Simons K, Verkade P (2003) *FEBS Lett* 538:85–88.
38. Parton RG (1995) *J Histochem Cytochem* 43:731–733.